FEASIBILITY OF USING A HAND-HELD SCANNER FOR PROVIDING LOWER COST 3D IMAGING FOR MAXILLOFACIAL PROSTHETICS

G.M. Barnard[1*] & J.G. van der Walt[2]

[1]Department of Design and Studio Art,
Central University of Technology, Free State, South Africa
gbarnard@cut.ac.za

[2]Department of Mechanical and Mechatronics Engineering
Central University of Technology, Free State, South Africa
jgvdwalt@cut.ac.za

ABSTRACT

Maxillofacial prosthetics, a specialized branch of prosthetic care, may not always be capable of restoring a missing facial feature's function but aims to create a more normalized facial appearance through ever-evolving techniques and technologies. Despite CT and MRI having considerable advantages in acquiring reliable dimensional form and sizes of affected areas needed for designing a prosthesis through additive manufacturing, it is not without complications. One key drawback is the high costs involved and how this excludes a significant number of sufferers from gaining access. This study aimed to investigate if a state-of-the-art three-dimensional (3D) portable scanner used in healthcare and engineering industries (Artec® Spider®) can be used to generate external medical digital data suitable for the fabrication of maxillofacial prostheses. Results from the study showed that the scanner produces scans that are comparable in accuracy to that of CT scanner but at much lower cost. This enables a more significant number of patients who require maxillofacial prosthetic care to be helped.

[1] The author is enrolled for an M Tech (Design) degree in the Department of Design and Studio Art at Central University of Technology, Free State

1. INTRODUCTION

The loss or absence of facial features can be devastating to the social wellbeing of a patient. This may result from several causes such as trauma, burns, disease or congenital disorders. Regardless of the causes, the psychological implications on the sufferer could be as debilitating as the physical leading to lower self-esteem and a diminished quality of life [1], [2].

The traditional process of fabricating a facial prosthesis such as an ear, involves taking a negative impression of the opposite ear using an impression material such as water-based alginate. The impression is then used to cast a positive of the ear in plaster and this is then used as example to sculpt the missing ear in wax. The wax model is next invested in plaster, the wax is molten out and bio-compatible silicone is cast into the plaster mould to create the prosthesis. This technique requires significant skill from the technologist sculpting the prosthesis in wax and is time consuming. Taking an impression to produce a nose prosthesis is furthermore a risky undertaking since the impression material may enter the patient's airways which may lead to suffocation. Many patients experience taking an impression in the facial area as traumatic and some may furthermore experience an allergic reaction to the impression material. Facial silicone prosthetics have a limited lifespan and therefore need to be replaced regularly. Each time a new impression needs to be taken of the patient since the facial features of the patient changes over time. The weight of the impression material furthermore deforms the soft facial tissue of the patient during the impression taking procedure. This often results in a less than ideal fit of the final silicone prosthesis.

In recent times, emerging technologies have begun to establish a presence in maxillofacial prosthetic fabrication through combinations of Magnetic Resonance Imaging (MRI), Computerized Tomography (CT), Computer-Aided Design (CAD) and various Additive Manufacturing (AM) processes. The scanning technologies are precise and reliable for acquiring dimensional data while AM produces accurate artefacts in short lead times [3], [4].

CT imaging, which is most commonly used to determine facial geometry, present the advantage of non-contact with the patient. The patient therefore experiences less trauma and the geometry is determined accurately without the risks and problems associated with impression material. The output format for CT is Digital Imaging and Communications in Medicine (DICOM) which need to be translated to Standard Triangulation Language (STL) format to make it suitable for AM technologies. Different software packages are available for this purpose such as Mimics® from Materialise®. Once the scan data is converted to STL format, the scan images can be manipulated as required. In the case of a missing ear, the healthy opposite ear can easily be mirrored about the mid-plane of the patient's head in the virtual environment using a software package such as Magics®, also from Materialise®. A negative mould can be designed in Magics® and printed using a variety of AM technologies. This technique has been reported on by a number of authors [5 - 11].

Despite CT having considerable advantages in acquiring the geometry of the affected area needed for designing a prosthesis, it is not without drawbacks. One key concern is the high costs involved in having a CT scan taken and how this excludes a significant number of patients from gaining access. Unfortunately, this is especially the case in South Africa, where a large proportion of the population is dependent on the government for health care assistance [12], [13]. The use of an alternative, inexpensive methods of digital data capturing could be implemented as a means of delivering lower-cost assistance for maxillofacial prosthetic fabrication.

The aim of this study was to investigate if a three-dimensional (3D) hand-held scanner can generate sufficiently accurate digital data suitable for the fabrication of maxillofacial prostheses. The use of such a portable 3D scanner should be able to generate external medical digital data that is more cost-effective in comparison to CT imaging. By contributing to the lower cost for the generation of such digital data, it can potentially provide access to a more significant number of patients who require maxillofacial prosthetic care. The study furthermore aimed to evaluate the use and capabilities of alternative software packages to process raw CT image data into digital models needed for an AM process as a means of lowering facial prosthetic costs.

Although numerous low cost hand-held scanners are now available commercially, high scanning resolution is required to scan intricate anatomical features such as ears to produce prostheses. An Artec® Spider® hand-held scanner was available to the research team and was used in this study (Figure 1). This is a state-of-the-art structured light 3D hand-held scanner used in healthcare and engineering industries. It has a resolution of 0.1 mm with a working distance of 170 – 300 mm and a cost of about US$ 25 000.

Figure 1: Artec® Spider® hand-held scanner.

In order to compare the scanning ability of the Spider® scanner to a CT scanner, a test artefact needed to be designed and produced. A literature search presented few examples of designed artefacts for the sole purpose of measuring scanning accuracies. Elements from research evaluating the accuracy of AM processes were therefore assessed and adapted for the test artefact in the current study.

Kruth made one of the earliest attempts in designing a benchmark artefact for studying layer manufacturing technologies. In his design, he used squares, embossed letters, cylinders, inclines, overhangs, and an inverted U frame to create an artefact capable of being measurable in all three directions (Figure 2a). The model's dimensions are relatively small compared to most AM device's building platforms and possessed no repeated design features. This was due to the initial intention behind the model which was to determine the accuracy of a particular AM device over a series of repeated copies. The used orientation of the artefact, dimensions and printing resolution were selected to reduce production time [14].

In their research to determine variables affecting machine parts' accuracy, Cook and Soons used a circle-diamond-square test part with an inverted cone that is commonly used to evaluate the five-axis performance of milling machines (Figure 2b). The test artefact was based on the classic Aerospace Industries Association (AIA), National Aerospace Standard, NAS 979 circle-diamond-square with an inverted cone. The several tests features making up the artefact was intended for measuring size, flatness, squareness, parallelism, and surface finishes. The features consisted of a squared shape rotated at 45° and intended for measuring size. A ramping feature with a 5° incline was included for defining angular deviation. The center circle was used for determining circularity, size and surface finish. Lastly, an inverted cone feature was additionally included to help further facilitate Computer Numerical Control (CNC) machining's performance evaluation [15].

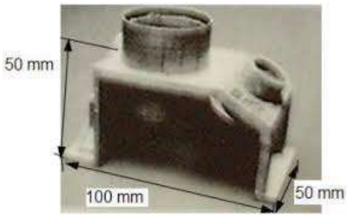

a

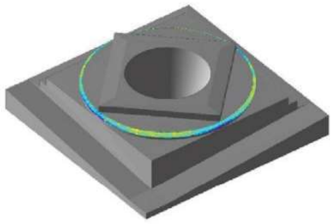
b

Figure 2a: Design of additive manufacturing testing models by Kurth and Cook, Figure 2b.

In attempting to produce a standardized artefact for evaluating AM processes, Moylan suggested that several considerations be made before initiating the design process (Figure 3a). Firstly, the artefact should be large enough to measure the AM's performance near the model's edges and centered areas. Secondly, the artefact should possess numerous small, medium, and large features. Thirdly holes and bosses (protruding features) should be present to help verify beam width compensation. Lastly, the artefact's fabrication should not consume a large quantity of material or time and be easily measurable [16].

To determine shrinkage and accuracy changes during the indirect laser sintering of the aluminum process and understand the underlying factors that affect tolerances inspired the artefact design by Sercombe and Hopkinson (Figure 3b). Their design used a square base with two staircases with uniform thickness, orientated along both the X and Y planes. One drawback of this design was that it could only determine linear accuracy and require numerous manufactured copies to determine accuracy [17].

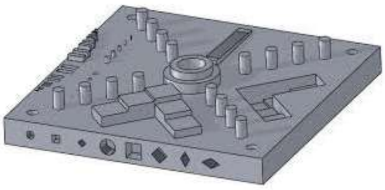
a

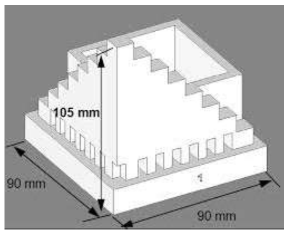

b

Figure 3a: Design of test models by Moylan and Sercombe, Figure 3b.

2. METHOD AND MATERIALS

2.1 Design and fabrication of a test artefact

The design, fabrication, and evaluation processes of the test artefact in the current study were divided into three stages:

The first stage entailed establishing a design criterion that identified and demonstrated necessary elements and factors that should be implemented in the designs of a test artefact. These were gained from a literature review of research material where geometric test models were used to determine AM processing accuracy as descibed above. Specific features to highlight the limitations of CT scanning as well as optical scanning were also considered and incorporated into the design. This included for example the inability of the Spider® scanner to scan overhangs and undercuts and problems experienced by CT scanners to scan metal objects that may be present in the scanning field. After establishing the design criterion, a series of individual developmental test artefacts were produced and subsequently combined into a single digital geometry.

The second stage focused on the fabrication and evaluation of the first test artefact design. For this, the prototype's digital format was converted into an STL format and was produced in nylon PA2200 on an Electro Optical Systems (EOS) P380 laser sintering system. After fabrication, it was presented to a group of experts who evaluated if the prototype had met all the requirements put forward in the design criteria. From this, the decision was made that additional elements sould be included in the design criteria for a test artefact.

The third stage centered on designing and fabricating a revised second test artefact. All suggestions put forth through deliberations with experts were incorporated into this second design iteration. Upon recommendations, certain test features were modified while additional anatomical test features were added (Figure 4).

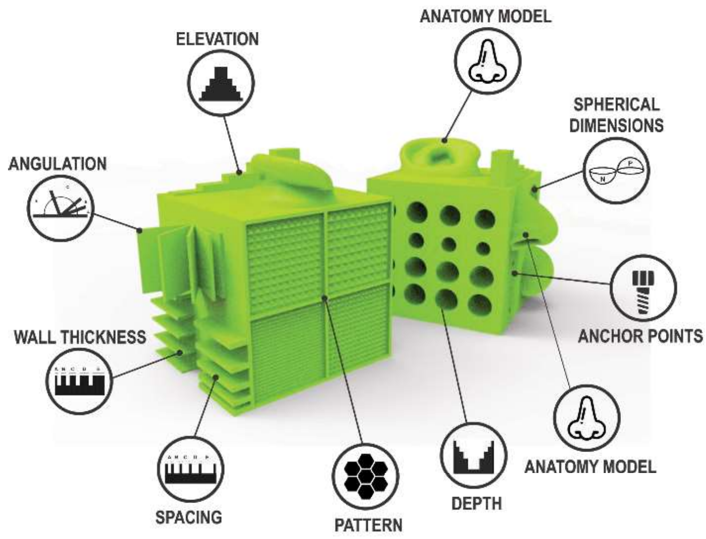

Figure 4: Design of final test artefact with elements.

Three metallic pins were also included in the design to represent the pins that are implanted into a patient's scull to retain an ear prosthesis. These pins will be present when the patient is scanned to produce a replacement prosthesis. After completing the design, the final test artefact was prepared for the AM process as before by converting its digital format to STL and then printing on an EOS P380 laser sintering machine in nylon (Figure 5).

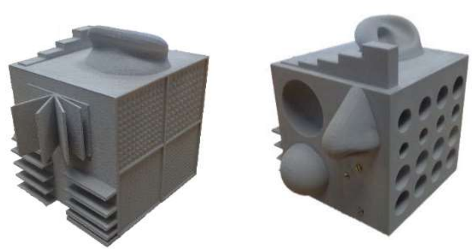

Figure 5: Final additive manufactured test artefact.

2.2 Hand-held scanning of the test artefact

Next, geometric data capturing of the artefact created in the design and fabrication phases was performed. The scanning process took place in a standard office cubicle using the Artec® Spider® hand-held scanning device with the artefact positioned on a rotational platform. In total, 71 scans were captured of the test artefact. Each scan was scrutinized, and many were eliminated because of either too low scan quality or not enough common geometric features visible which is required to align the scans. Based on this, the number of scans was reduced to 37, which were imported into Artec® Studio® software which is available to Artec® scanner users. The Artec® Studio® software allows for each scan's preparation by erasing irrelevant geometries, aligning, closing gaps and combining meshes into a single digital 3D model which can be exported as a STL file. The software also allows the digital 3D model to be simplified by reducing the number of polygons making up its digital surface to produce smaller file sizes. Figure 6 shows the scanning and processing steps.

Figure 6: Hand-held scanning process of the test artefact.

2.3 CT scanning of the test artefact

A CT scan of the test artefact was performed at the Oncology Department of National Hospital in Bloemfontein. Various sets of cross-sectional DICOM image slices were produced at 0.5 mm which was the finest scanning resolution possible on the available Toshiba Aquilion LB® CT scanner. Thereafter, the raw DICOM data was uploaded to three selected software applications, namely Mimics®, 3D Doctor® and Invesalius® as shown in Figure 7.

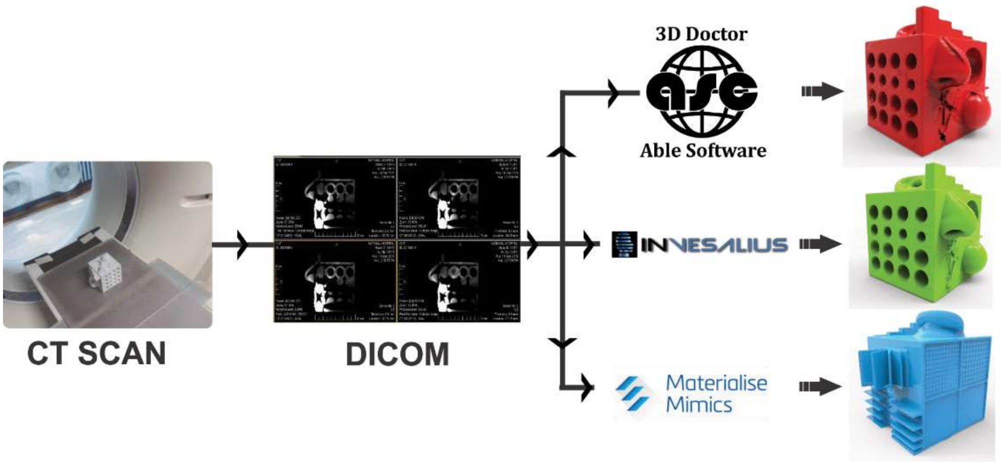

Figure 7: Scanning and processing the test artefact.

Mimics®, was chosen for having a well-proven track record and is generally regarded as a world leader generating high-quality 3D models from various medical scanning modalities. Mimics® is however the most expensive of the three translation software packages considered and can cost up to US$100,000 per seat [18]. The second selected software, 3D Doctor® is commercially available at a much more reasonable price of US$4800 per license. The third selected software, Invesalius® is open source-based and can thus be downloaded for free from the internet. The rationale behind choosing the last two mentioned software packages was to gauge the technological differences between what is commonly used, what is available at low cost and free of cost. Although differently priced, the software makes use of similar methods in processing the DICOM data into digital STL 3D models. These included using the Hounsfield scale to increase or decrease contrasts within DICOM images to define boundaries or regions of interest from unnecessary or irrelevant scan data and afterward applying this to each image within the image stack.

2.4 Micro-CT scanning of the test artefact

In the final phase of the study, the various digital 3D models produced through hand-held scanning and CT images translated through the three mentioned software packages needed to be compared to quantify differences. To achieve this, a digital benchmark model of the final test artefact had to be generated from the highest scan quality and accuracy available that reflected the exact physical sizes of the printed test model. The test artefact was subjected to a micro-CT scanning procedure using a Mediso® NanoScan® Micro CT scanner at the Nuclear Energy Corporation of South Africa (NECSA) to produce a digital 3D model (Figure 8) which was considered as gold standard in the study.

Figure 8: Digital 3D model produced through Micro CT scanning of test 3D printed test artefact.

Similar to medical CT scans, metal objects create scatter artefacts in the micro-CT scanner's immages. It was therefore decided to remove the three metal pins representing implant retension anchors from the test artefact to create an accurate scan. The scan model and those produced through the hand-held and CT scanning procedures were then digitally compared through myVGL software from Volume Graphics in collaboration with the Stellenbosch University's Central Analytical Facility. The comparrisons were performed by comparing volumetric sizing and using deviation analysis maps.

3. RESULTS AND DISCUSSION

3.1 Evaluation of scans performed with the hand-held scanner

The STL file of the scanned test artefact was uploaded into 3D viewing software and the following visual observations were made with reference to Figure 9. (see Figure 4 for description of specific test geometry features)

- The elevation test geometry showed no visible difference in geometry on all five elevations, except the top elevation, which showed a small misalignment at its side (A).

- As expected, the scanner did not perform well in scanning deep or small diameter holes in the Depth test. The scanner works on a line of sight principal where there is an angle between light projected from the camera and images captured by the camera. There is therefore a limit to the depth of a cavity that can be scanned since the edges of the cavity obscures the view of the bottom of the cavity at an angle. Conical holes which were included in the design scanned better compared to holes with straight walls. The feature best captured in the depth test was one of the holes with walls set at an angle of 21 degrees (B).
- In the pattern test geometry, the four squares with variously sized patterns were captured at a high precision showing no areas of missing or badly defined geometries (C).
- For the Anchor point test geometry, all three metallic inserts embedded into the test artefact were captured although some detail was lost (D). This is because reflective surfaces do not scan well.
- In the Angulation test geometry, all features positioned at various degrees were all captured sufficiently except for the corners with a pitch of 10 and 20 degrees respectively. These were fused towards the centre in an attempt by the software to create a “watertight” mesh (E).
- The Anatomical test geometry features were captured successfully without any holes caused by the intricate overhangs or undercuts of the geometries (F).
- The Spherical test geometry features displayed no visual deformation on either impression or depression test features (G).
- The Wall thickness and Spacing test geometry features presented some minor distortion. Some edges of the elements in the Wall thickness test geometry model twist upwards, while the smallest spacing in the Spacing test geometry were closed in an attempt by the software to repair the model's digital mesh, which is very similar to result from the Angulation test feature’s results (H).

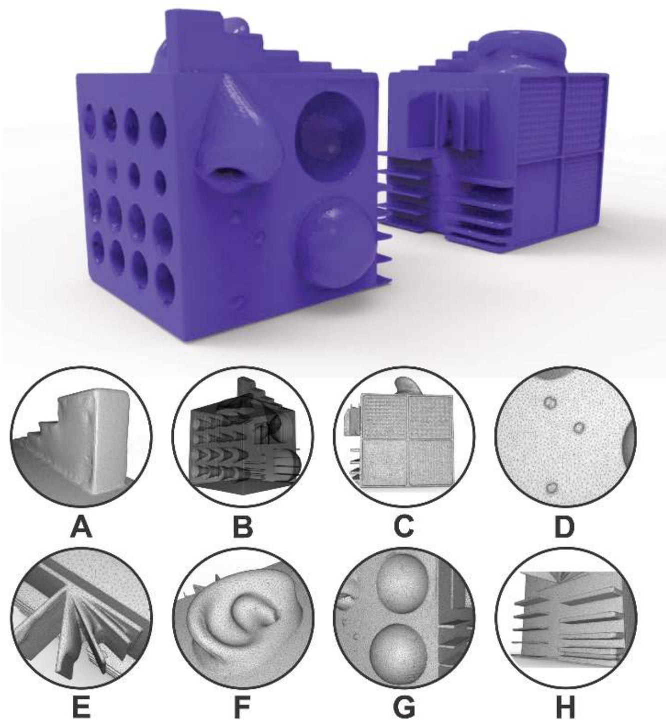

Figure 9: Result of hand-held scanning the final test artefact.

3.2 Evaluation of scans performed with CT scanner translated with different software packages

The following visual observations were made from the 3D models generated by 3D Doctor®, Mimics® and Invesalius® from CT scans of the test artefact (with reference to Figure 10):

- The Anchor point test feature, which included three metallic inserts representing an area where a prosthesis could be attached, showed distortion and missing surface geometry in all three STL models. In this regard, Mimics® (B1) produced a better result followed closely by Invesalius® (C1) and lastly 3D Doctor® (A1).

- The Anatomical Test model feature of the "nose" appeared to possess a slight defect present in all 3D models to varying degrees. The nose's bridge seems to have acquired some additional thickness, stretching from the nose's tip to where it connects to the main body. The Mimics® digital model (B2) possessed the least amount of deviation followed closely by Invesalius® (C2) and lastly 3D Doctor® (A2).

- The Spherical test model showed no visible deviation in the impression feature; however, the depression feature did show some flaws in the models from Invesalius® (C3) and 3D Doctor® (A3). In both these models, additional surface geometry was observed stretching from the centre of the protruding sphere to the top where it attaches to the main body. This appears to be similar to the results from the anatomical test feature. Regarding performance, the Spherical test model features from Mimics® (C2) performed best-followed closely by Invesalius® and lastly 3D Doctor®.

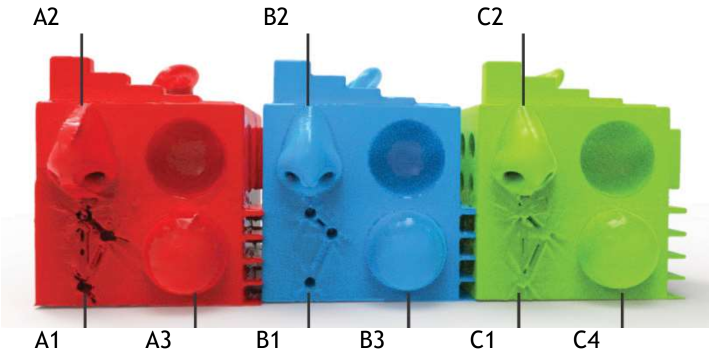

Figure 10: CT Results of Anchor point (3D Doctor® A1, B1, C1), Anatomical (Mimics® A2, B2, C2) and Spherical (Invesalius® A3, B3, C3) Test Features.

- The Depth test (Figure 11), features were generated correctly across all three software packages. The various depth, radius, and diagonal pitch of individual holes were displayed without any visual deviations. This was expected since the CT scanning is not restricted by undercuts or overhangs in test models when scanning such as with optical scanning.

A B C

Figure 11: CT Results of Depth Test Features for 3D Doctor® (A), Mimics® (B) and Invesalius® (C).

- One of the more noticeable differences between the various 3D models was observed in the Pattern test feature (Figure 12). The 3D model produced through the Invesalius® (C) software package performed the best, displaying all four the pattern grid sizes clearly. However, the smallest grid pattern of 2 mm x 2 mm in size was not that well defined. The second-best result was from Mimics® (B), which accurately displayed the two larger grid patterns but struggled with reproducing the smaller 3 mm x 3 mm and 2 mm x 2 mm sized patterns. The 3D Doctor® (A) model's result was similar to that of Mimics® with the larger two grid patterns displayed clearly while the finer grid patterns appeared smoothed.

A B C

Figure 12: CT Result of Pattern Test Features for 3D Doctor® (A), Mimics® (B) and Invesalius® (C).

- The Angulation test feature (Figure 13) was generated correctly by Mimics® (B1) and Invesalius® (C1) but in the 3D Doctor® model (A1), the 10° corner's surface geometry appears to have been fused closed.
- The Wall Thickness and Spacing test features have been generated sufficiently except for some minor warping on the fin structures' edges. The Invesalius® model (C2) showed the least amount of deviation followed by Mimics® (B2) and lastly 3D Doctor® (A2) software package (Figure 13).

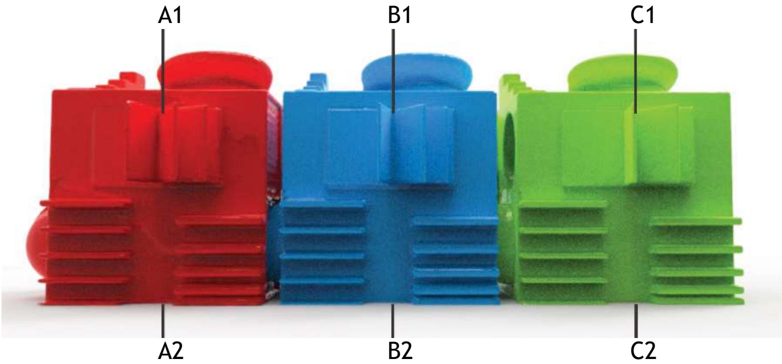

Figure 13: CT results of Angulation Test Features: 3D Doctor® (A1), Mimics® (B1), Invesalius® (C1), Spacing and Distance Test Features: 3D Doctor® (A2), Mimics® (B2), Invesalius® (C2).

- The Elevation Test feature (Figure 14) was generated correctly across all three 3D models. The Anatomical test feature of an ear was also generated sufficiently without any visual deviations or errors due to undercuts or overhangs (Figure 16).

A B C

Figure 14: CT Result of Elevation Test Features and Ear for 3D Doctor® (A), Mimics® (B) and Invesalius® (C).

3.3 Comparison between scans performed with the hand-held scanner and CT scanner to scans performed with micro-CT scanner

Two methods were used in comparing scans from the hand-held and CT scanner (translated through different software packages) to scans from the micro-CT scanner. In the first method of comparison, the digital models' volumetric sizing was calculated and displayed in relation to the size of the micro-CT scanned 3D-printed test artefact as gold standard. For the second method, a deviation map displaying various colours when two models are digitally superimposed on top of one another for comparison was used. These colours correspond to the amount of deviation between the models' dimensions. Areas displaying colours ranging from green to red indicate that particular areas are larger. In contrast, colours ranging from green to magenta show areas that are smaller.

3.3.1 *Comparisons between CAD and Micro-CT STL models*

In order to determine how accurately the test artefact was produced, the CAD design of the artefact was compared to the micro-CT scan of the 3D printed artefact. After generating a digital model from the micro-CT image data, both the CAD and micro-CT STL models were uploaded to the myVGL® software application. Digitally superimposing the models on top of one another showed that the model generated through the micro-CT scan was slightly larger (3.31%) in volume with deviation in measurements shown along the X, Y, and Z-axes (Figure 15).

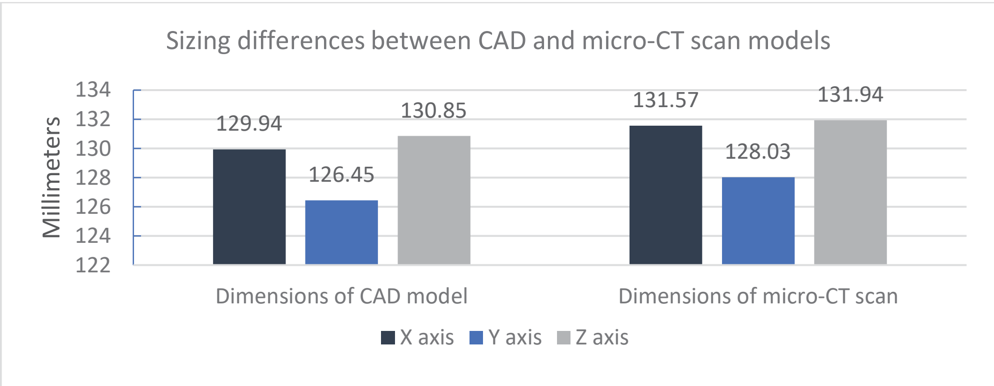

Figure 15: Comparison of dimensions between CAD and micro-CT scan models.

The differences in dimensions are displayed through the colour tones ranging from yellow to red shown in the deviation analysis image map (Figure 16). Areas is green was a match to the dimensions of the original CAD model.

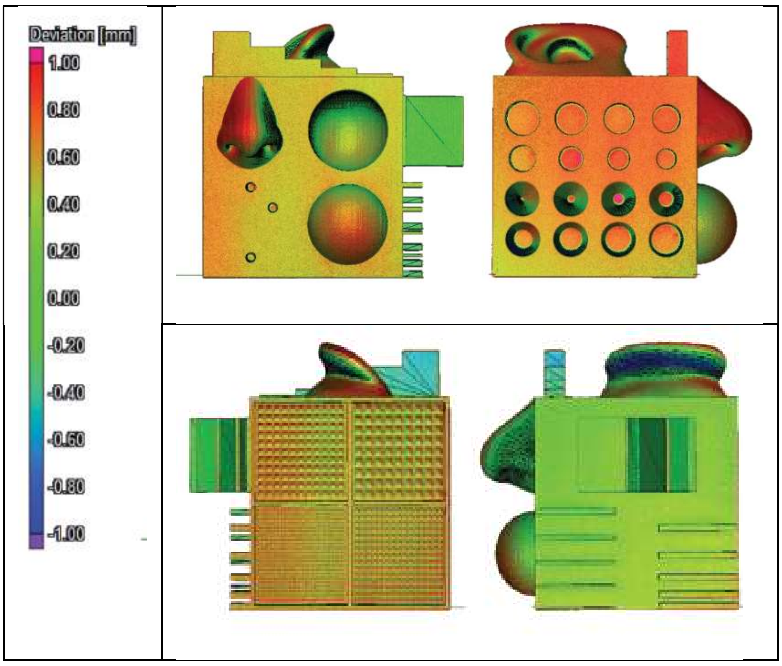

Figure 16: Deviation map between CAD and micro-CT scan models.

3.3.2 Comparisons between hand-held and micro-CT scan models

The second comparison was between the STL model produced from the Artec® Spider® hand-held scanning device and the micro-CT scan model of the 3D printed test artefact. Through software analyses, it was shown that the STL model generated from the hand-held scanner was slightly smaller than that of the micro-CT, with a volumetric difference of 0.42% (Figure 17).

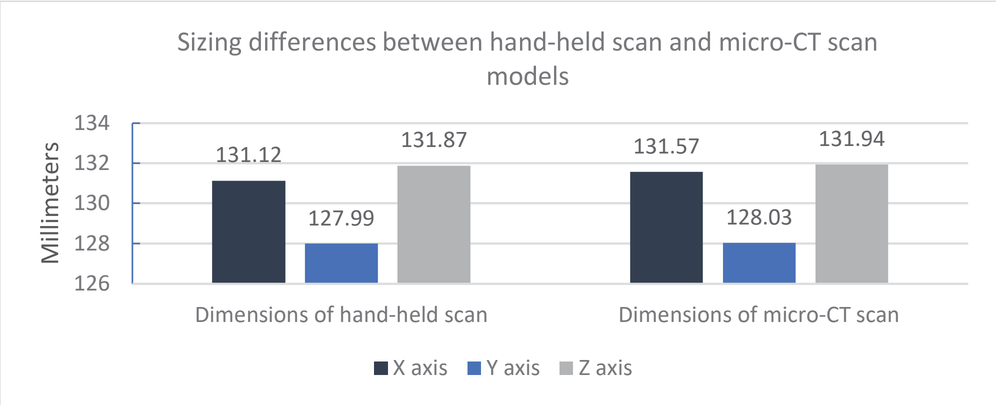

Figure 17: Size differences between Artec® Spider® and micro-CT scan models.

Other variations in both the depth, angulation, and distance test features were also observed. These were the result of overhangs and undercuts restricting the line of sight of the hand-held scanner. These differences are displayed in colours ranging from dark magenta to red glow in the deviation analysis image (Figure 18). Most prominent deviation can be observed inside the holes of the depth test features. Since the metallic pins were removed from test artefact during micro-CT scanning, the three positions show large deviation which is not actually the case.

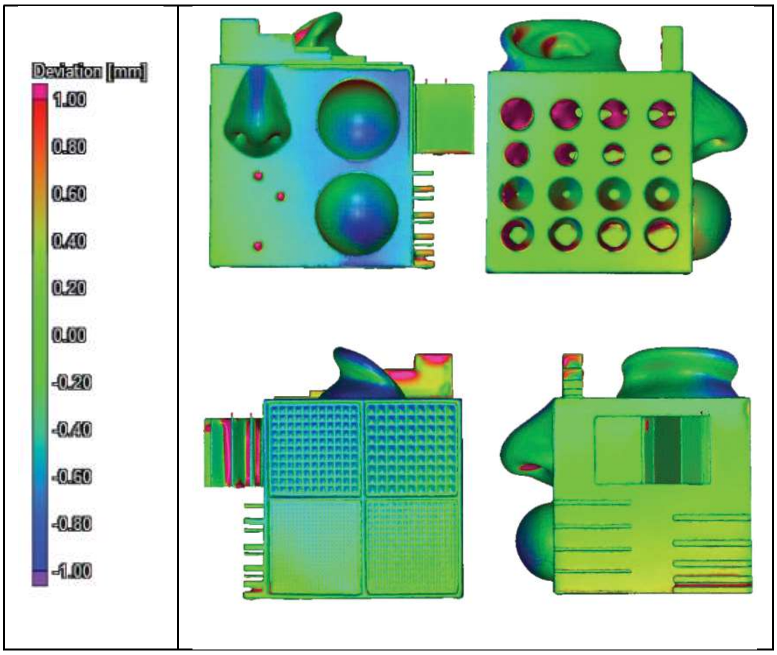

Figure 18: Deviation map between hand-held scan and micro-CT scan models.

3.3.3 Comparisons between micro CT and 3D Doctor® STL models

For the third comparison, the STL model generated from medical image translation software application 3D Doctor® was compared against the micro-CT scan model. The comparison showed that 3D Doctor® model was slightly smaller than that of the micro-CT, with a volumetric difference of 4.05% (Figure 19).

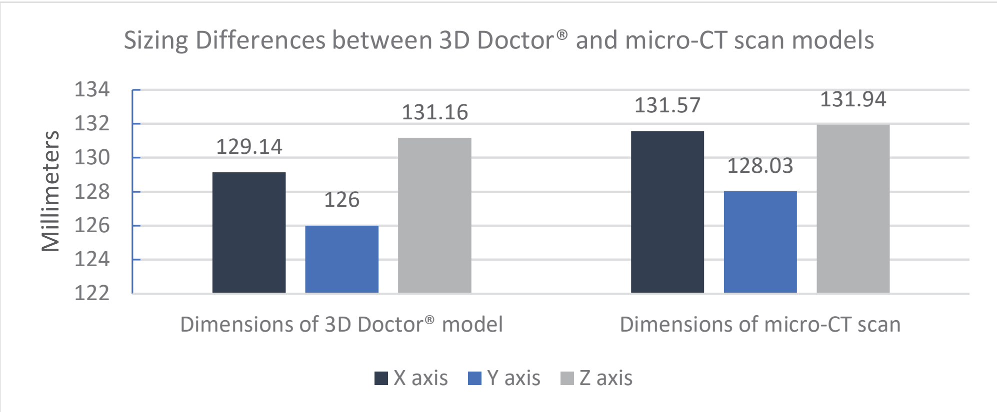

Figure 19: Size differences between 3D Doctor® and micro-CT scan models.

In the deviation analysis image map, the first apparent visual difference is the presence of deformations around the area with the metallic inserts because of X-ray scattering during CT scanning. Another visual difference was the absence of more delicate details of the Pattern test feature. The smallest areas appear to be smoother than the larger patterns, with some additional shrinkage indicated by the colour magenta (Figure 20). Additionally, no deviations were found with the depth, angulation, or distance test features, as in the case with the hand-held scanner's model. This is due to the CT scanner's ability to capture data regardless of intricate overhangs, undercuts, or other visual obstructions of areas.

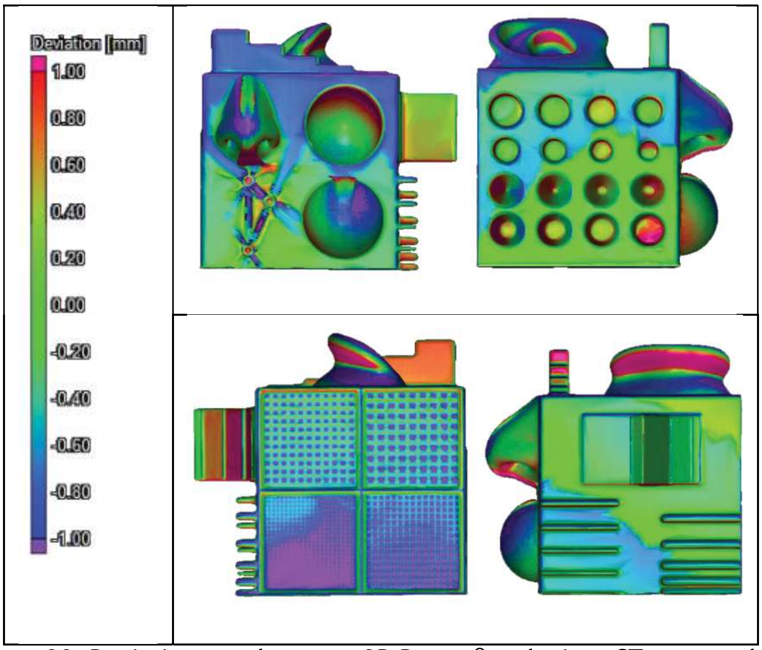

Figure 20: Deviation map between 3D Doctor® and micro-CT scan models.

3.3.4 Comparisons between Micro CT and Invesalius® STL models

In the fourth comparison, Invesalius® was the second software application to be compared, which made use of CT scanning and DICOM translation to produce a 3D model. As with the previously created STL models from both CT and hand-held scanning, the Invesalius® model appeared smaller, with a volumetric difference of 4.20% (Figure 21).

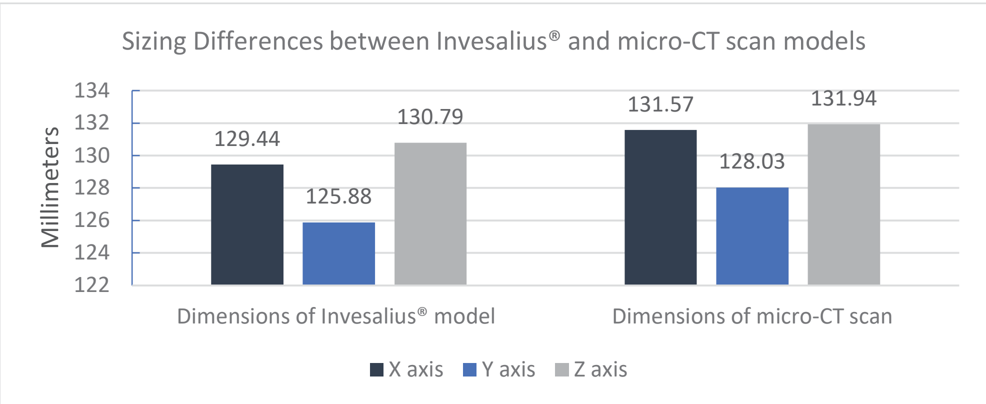

Figure 21: Size differences between Invesalius® and micro-CT scan models.

Visually inspecting the deviation analysis image map, the first apparent difference was disturbances and missing mesh geometry surrounding area with the metallic inserts in the Anchor Point test geometry (Figure 22). The Pattern test features appear to be more prominent and more clearly defined than the 3D Doctor model, displaying all four grid patterns sizes, although slightly smaller in size, as indicated by the colours cyan to dark blue.

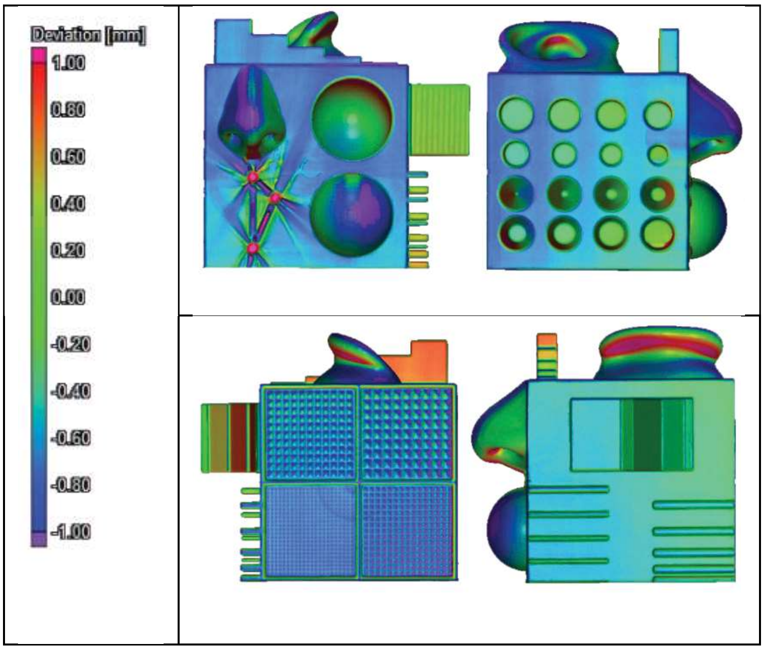

Figure 22: Deviation map between Invesalius® and micro-CT scan models.

3.3.5 Comparisons between micro-CT and Mimics® STL models

In the fifth comparison, the STL from the Materialize® Mimics® software package was compared against the micro-CT scan. As with all other compared STL models, this model appears somewhat smaller, with a volumetric difference of 5.00% (Figure 23).

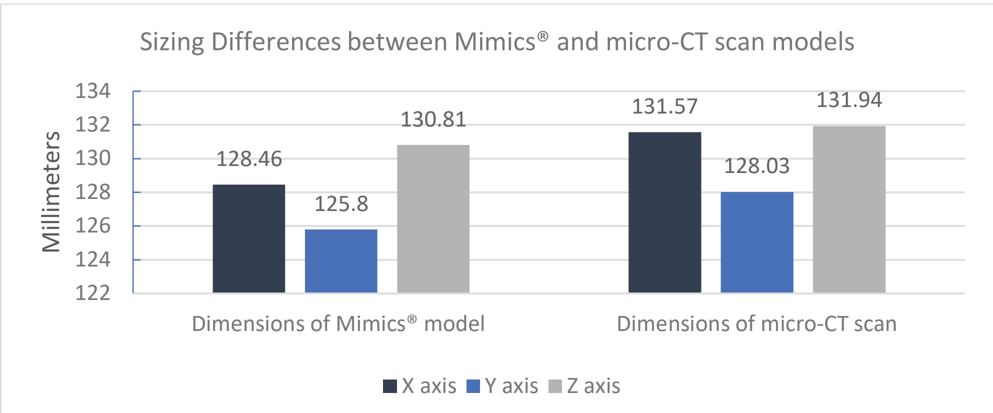

Figure 23: Size differences Mimics® model and micro-CT scan models.

Upon visual analysis, one can clearly distinguish all the finer geometries in the pattern test, to a greater extent than those shown in the 3D Doctor® model, although similarly undersized as the Invesalius® 3D model (Figure 24). Other features are very clearly defined, except for missing surface data around the Anchor point test feature, similar to previous comparisons.

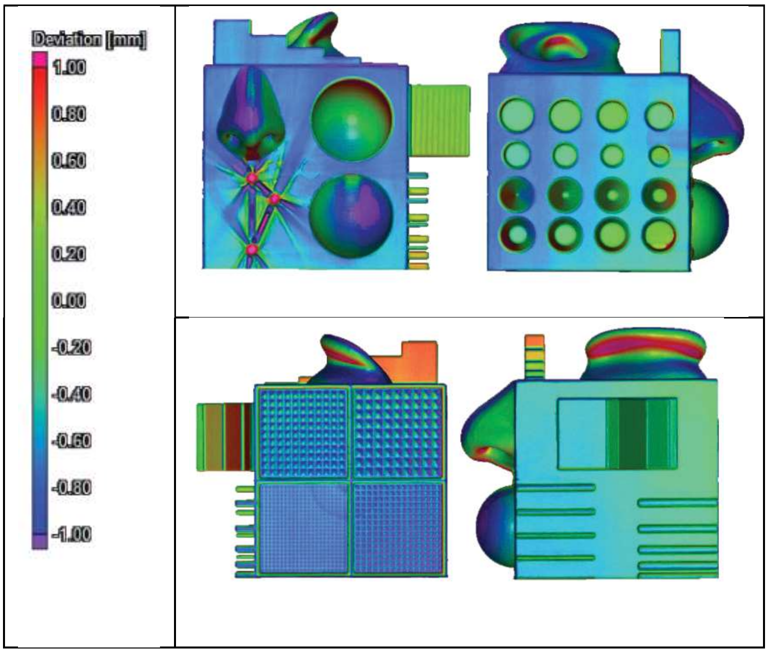

Figure 24: Deviation map between Mimics® and micro-CT scan models.

4. CONCLUSION

The aim of this study was to investigate if a hand-held scanner can generate sufficiently accurate digital data for the fabrication of maxillofacial prostheses instead of using expensive and CT scanning to which many patients have limited access. The study furthermore aimed to evaluate different software packages to process raw CT image data into digital models required for producing prostheses through AM process as a means of lowering facial prosthetic costs. Results from the study point in favour of a hand-held scanner as a valuable, affordable tool in a small maxillofacial prosthetic unit to capture digital geometric data of patients. Although there are limitations to the ability of the scanner to scan areas with overhangs and undercuts, the accuracy of scans is comparable and, in some cases, even better than that of a CT scanner. Developing a scanning protocol that demonstrates the proper methods of capturing facial features of patients using a hand-held scanning device should lessen restrictions due to undercuts and overhangs. Considering various free to lower-cost DICOM medical image translation software applications should also be taken into consideration as a means of lowering the cost of generating digital 3D models either for viewing or prosthesis fabrication through additive manufacturing.

5. ACKNOWLEDGEMENTS

The financial support from the South African Research Chairs Initiative of the Department of Science and Technology and National Research Foundation of South Africa (Grant № 97994) and the Collaborative Program in Additive Manufacturing (Contract № CSIR-NLC-CPAM-15-MOA-CUT-01) is gratefully acknowledged. Thanks also to the Centre of Rapid Prototyping and Manufacturing (CRPM) and Stellenbosch University's Central Analytical Facility for technical support.

REFERENCES

[1] **Hatamleh, M. M., Haylock, C., Watson, J., & Watts, D. C.** (2010). Maxillofacial prosthetic rehabilitation in the UK: A survey of maxillofacial prosthetists' and

technologists' attitudes and opinions. *International Journal of Oral and Maxillofacial Surgery*, 39(12), 1186–1192

[2] **Neuman, M., Baura, G., Meldrum, S., Soykan, O., Valentinuzzi, M., Leder, R., Zhang, Y.-T.** (2012). Advances in Medical Devices and Medical Electronics, (2014). Available from: https://doi.org/10.1109/JPROC.2012.2190684, Accessed on 4 September 2020

[3] **Dincă, L. L., Banu, A., & Vişan, A.** (2017). Additive manufacturing in maxillofacial reconstruction. MATEC Web of Conferences, 137, 02001. Available from https://doi.org/10.1051/matecconf/201713702001, Accessed on 2 September 2020

[4] **Tsuji, M., Noguchi, N., Ihara, K., Yamashita, Y., Shikimori, M., & Goto, M.** (2004). Fabrication of a maxillofacial prosthesis using a computer-aided design and manufacturing system. *Journal of Prosthodontics*, 13(3), 179–183

[5] **Watson, J., Hatamleh M. M.** (2014) Complete integration of technology for improved reproduction of auricular prostheses, *J. Prosthet. Dent.*, vol. 111, no. 5, pp. 430–436

[6] **Liacouras P., Garnes J., Roman N., Petrich A., Grant G. T.** (2011) Designing and manufacturing an auricular prosthesis using computed tomography, 3-dimensional photographic imaging, and additive manufacturing: A clinical report, *J. Prosthet. Dent.*, vol. 105, no. 2, pp. 78–82

[7] **Subburaj K., Nair C., Rajesh S., Meshram S. M., Rapid B. R.** (2007) Rapid development of auricular prosthesis using CAD and rapid prototyping technologies, *Int. J. Oral Maxillofac. Surg.*, no. 36, pp. 938–943

[8] **Wang S., Leng X., Zheng Y., Zhang D., Wu G.** (2015) Prosthesis-guided implant restoration of an auricular defect using computed tomography and 3-dimensional photographic imaging technologies : A clinical report, *J. Prosthet. Dent.*, vol. 113, no. 2, pp. 152–156

[9] **Mohameda N. A., Rajion Z. A.** (2015) Prosthetic ear reconstruction applying computer tomographic (CT) data and additive manufacturing technologies, *J. Teknol.*, vol. 76, no. 7, pp. 63–68

[10] **Çötert H. S.** (2015) Stereolithographic rapid prototyping of ear prostheses, *Int. J. Appl. Dent. Sci.*, vol. 1, no. 4, pp. 64–67, 2015.

[11] **Ferreira R., Vives P.** (2019) Two auricular epithesis surgical cases retained by a custom titanium implant: result at four years," J. *Stomatol. Oral Maxillofac. Surg.*, vol. 120, no. 2, pp. 147–151

[12] **Coovadia, H., Jewkes, R., Barron, P., Sanders, D., & McIntyre, D.** (2009). The health and health system of South Africa: Historical roots of current public health challenges. *The Lancet*, 374(9692), 817–834

[13] **Kautzky, K., & Tollman, S. M.** (2008). A Perspective on primary health care in South Africa. South African Health Review, 17-30. Available from : https://doi.org/www.hst.org.za/uploads/files/chap2_08 Accessed on 9 September 2020

[14] **Kruth, J.** (1991). Material Increases Manufacturing by Rapid Prototyping Techniques. *Annals of the CIRP*, 40, 603–614

[15] **Cooke, A & Soons, J.** (2010). Variability in the Geometric Accuracy of Additively Manufactured Test Parts. In *21st Annual International Solid Freeform Fabrication Symposium* (pp. 1–12).

[16] **Moylan, S., Slotwinski, J., Cooke, A., Jurrens, K., & Donmez, M. A.** (2014). An Additive Manufacturing Test Artifact. *Journal of Research of the National Institute of Standards and Technology*, *119*, 429–459.

[17] **Sercombe, T., & Hopkinson, N.** (2006). Process Shrinkage and Accuracy during Indirect Laser Sintering of Aluminium. *Advanced Engineering Materials*, 8(4), 260–264

[18] **Medical Design and Outsourcing** (2020). 3D printing can give your medtech startup a competitive edge, Available from https://www.medicaldesignandoutsourcing.com/3d-printing-medtech-startupedge/#:~:text=The%20dominant%20market%20player%20(Materialise,510(k)%2Dcleared%20version, Accessed on 4 October 2020.